



45S5/PEEK Coatings by Cold Gas Spray with In Vitro Bioactivity, Degradation, and Cellular Proliferation

Beatriz Garrido¹ · Vicente Albaladejo-Fuentes¹ · Sergi Dosta¹ · Natalia Garcia-Giralt² · Irene Garcia-Cano¹

Submitted: 2 October 2023 / in revised form: 23 November 2023 / Accepted: 17 January 2024 / Published online: 7 February 2024
© The Author(s) 2024

Abstract This study evaluated the biological response of cold-sprayed coatings composed of bioactive glass 45S5 and polyetheretherketone (PEEK). The functional coatings were produced by cold gas spray (CGS) technology, a technique that allows the deposition of powders at significantly low temperatures, avoiding heat damage to polymeric surfaces. By CGS, blends with different ratios of bioactive glass and PEEK powders have been deposited onto PEEK substrates to improve the response of the bioinert polymer. The bioactivity of the coatings when immersed in a simulated body fluid solution was evaluated by observation with scanning electron microscopy (SEM) and x-ray diffraction (XRD). Results verify that bioactive glass particles in the composite coatings enhance their bioactivity. A degradation test was performed with Tris–HCl solution. From the results obtained by inductively coupled plasma optical emission spectroscopy (ICP-OES) and the weight loss of the samples, it was noticed that the degradation was directly related to the amount of glass in the coatings. Finally, the ability of bone-forming cells to adhere and proliferate on the coatings was evaluated. These experiments showed that the presence of glass particles does not cause a significant increase in cell proliferation. Combining a bioactive material with PEEK leads to

forming a final component that provides suitable bioactivity to the final implant.

Keywords bioactive glass · bioactivity · cell proliferation · CGS · degradation behavior · PEEK

Introduction

Polyetheretherketone (PEEK) is a thermoplastic polymer with suitable mechanical properties for specific medical applications since this biomaterial is non-toxic and inert when implanted in the body. In the last decades, PEEK reached the market with good acceptance replacing common metallic biomaterials (stainless steels, cobalt–chrome alloys, and titanium alloys) (Ref 1, 2), mainly in spinal and dental applications (Ref 3). Nevertheless, using polymeric materials for biomedical applications is not only restricted to PEEK components. Since the late 1960s, ultra-high molecular weight polyethylene (UHMWPE) has been used in knee joint implants due to its great wear resistance and high fracture toughness. However, improving implant longevity remains a goal to increase the life quality of patients. In this respect, current research suggests that PEEK could be an alternative, providing better creep resistance and fatigue limit than conventional UHMWPE implants (Ref 4–6). Following the current trend, the use of PEEK in more implants could be considered in the coming years.

A vital aspect of the success of implants is their biological response, which is directly related to their bioactivity. In this sense, the main problem of PEEK as a biomaterial is the hydrophobicity and the lack of bioactivity, which is necessary to reach a good bonding between the implant and bone tissue (Ref 7). To date, several

✉ Beatriz Garrido
bgarrido@cptub.eu

¹ Department of Materials Science and Physical Chemistry, University of Barcelona, Martí i Franquès, 1, 08028 Barcelona, Spain

² CIBERFES, ISCIII, IMIM (Institut Hospital del Mar d'Investigacions Mèdiques), Doctor Aiguader 88, 08003 Barcelona, Spain

research studies have been performed to enhance the bioactivity of PEEK material, with most of the strategies focused either on the surface modification of the polymer (physical treatment, chemical treatment, or surface coating) or the preparation of a composite material with a bioactive element (Ref 8).

Bioactive glasses are biomaterials with high reactivity and degradability in body fluids. These glasses can bond to bone tissue by forming a biomimetic layer of hydroxy-carbonate apatite (HCA) on its surface. The presence of this HCA layer, with a composition similar to that of the bone, favors the good osteointegration of the implant to the bone matrix (Ref 9, 10). Different dissolution rates are obtained depending on the glass composition, which is more degradable for those glasses with a more open network (Ref 11). Bioactive glasses cannot be used as the primary material of an implant device due to their brittleness and very low fracture toughness. For this reason, their potential use is limited to non-load-bearing applications, such as coatings, graft bone, or scaffolds (Ref 12–14).

Different methods are available to deposit bioactive glasses onto materials with bio-inert behavior. However, in most of them, high temperatures are required, which can reduce bioactivity because it tends to crystallize (Ref 15, 16). For instance, enameling involves high temperatures to coat materials (Ref 17, 18), the sol–gel process needs a post-heat treatment (Ref 19, 20), and electrophoretic deposition requires conductive materials as coating or as substrate (Ref 21–23). Some works have used thermal spray methods to produce bioactive glass coatings, particularly atmospheric plasma spraying, and solution precursor plasma spraying (Ref 24, 25). However, these methods also involve high temperatures, a problem for coating polymeric surfaces.

A. Papyrin and coworkers developed cold gas spray (CGS) in the 1980s as a new thermal spray technique (Ref 26). This technique offers a fast coating deposition with low cost and high deposition efficiency. The deposition mechanism by CGS is based on supplying high kinetic energy to the coating feedstock particles. With this, deposition is achieved in two steps, the first step of particles adhesion to the substrate and the subsequent build-up of the deposit, which involve the plastic deformation of the particles due to the transformation of their kinetic energy into localized thermal energy when they impinge onto the substrate surface (Ref 27). The low processing temperatures used in CGS avoid the melting of the particles, which occurs in conventional thermal spray techniques (Ref 28–30). This feature can favor the deposition of glass materials without crystallizing them and polymers without decomposing them.

In the current work, we want to demonstrate CGS's capabilities for producing a composite biomaterial that

combines the mechanical properties of PEEK and the biological properties of bioactive glasses, with the ultimate aim of finally generating a functionalized biomaterial with an improved tissue response compared to PEEK implants.

For this, we developed PEEK/45S5 composite coatings on PEEK substrates by CGS. The bioactive glass used has the following composition: 45.0 SiO₂, 24.5 CaO, 24.5 Na₂O, and 6.0 P₂O₅ (wt.%) (Ref 31). It has been used previously as a composite material in combination with PEEK to produce coatings (Ref 32, 33), and it has been deposited by LPCGS for the first time in our previous work (Ref 34). To demonstrate the new solution's functionality, coatings with different amounts of glass were studied, analyzing the coating build-up, the microstructure, and the biological properties, particularly the ability to form an HCA layer, the degradation, and the cellular proliferation of osteoblasts on the coatings.

Material and Methods

Powder and Substrate

Two commercial powders were used to produce the composite coatings: a PEEK powder (Vitrex, UK) and a 45S5 bioactive glass powder (Denfotex Research, UK) produced by the traditional melt-quenching route.

The blends were prepared by manually mixing the powders. The proportions were chosen with a maximum of 50% glass by volume since the deposition efficiency was negatively affected when increasing the amount of glass in the blend. The blend ratios selected for spraying are listed in Table 1.

As the coatings were addressed to improve PEEK implants, the substrates used in all cases were of this material. PEEK disks with a 25-mm-diameter, cut from a PEEK bar (Vestakeep, Spain), were used to evaluate the cross-section of the coatings and the formation of an HCA layer. PEEK specimens obtained from a PEEK sheet (Ensinger, Spain), with an area of 8 × 8 mm and 5 mm

Table 1 Sprayed blends of PEEK and bioactive glass (v/v)

Blend/coating code%	Volume of PEEK%	Volume of 45S5%
PEEK 100	100	0
45S5 10	90	10
45S5 25	75	25
45S5 35	65	35
45S5 50	50	50

thick, were used for degradation test and biological characterization.

Powder and Coating Characterization

A scanning electron microscope (SEM) (Phenom ProX, Phenom-World BV, Eindhoven, The Netherlands) equipped with backscattered electrons (BSE) was used to characterize the morphology of the feedstock powders. Before the observation, both materials were coated with a gold layer to make them conductive using a sputtering coating system (E–5000, Polaron, Watford, England).

Both commercial powders were sieved using a 40- μm mesh sieve (Restch, Germany), and the fraction below this mesh was collected for producing the blends. The granulometry of the sieved powders was determined by a laser diffraction particle size analyzer (LS 13320, Beckman Coulter, California, USA).

Coatings were deposited using low-pressure cold gas spray (LPCGS) equipment (Dymet 423, Dycomet Europe, Akkrum, The Netherlands). The gun was equipped with a CK-20 nozzle. Air was used as the propellant gas with a gas pressure of 0.6 MPa. In this technique, the gas temperature is not very high. The equipment used allows us to work from room temperature to 500 °C, and the temperature used to produce the coatings in the study was between 300 and 350 °C. The stand-off distance was 10 mm, and all coatings were deposited by performing a single torch cycle.

Before the blend's deposition, PEEK substrates were grit-blasted (Formula 1400, Guyson International, Skipton, England) with corundum G24 (grit size 800 μm) at a pressure of 0.5 MPa. Afterward, samples were cleaned with ethanol. Suitable surface roughness is essential to favor the adhesion of particles to the substrate. In this study, grit-blasted PEEK roughness was $R_a = 4.9 \pm 0.4 \mu\text{m}$ and $R_z = 27.3 \pm 2.8 \mu\text{m}$. The surface roughness of the different coatings was measured to relate better the cell culture studies results with the coating's physical properties. The characteristic roughness values (R_a and R_z) were recorded using a surface roughness measurement device (Surftest 301, Mitutoyo, Kawasaki, Japan).

This study produced coatings with two different thicknesses by varying the traverse gun speed. To characterize the elements' deposition and distribution, thick coatings (around 800 μm) were sprayed using low traverse gun speed (80 mm/s). These coatings allowed a fair observation of the particle distribution throughout the coating and to see whether the distribution of the elements was equal at the interface with the substrate and the top of the coating. Conversely, thinner coatings (around 250 μm) were deposited, increasing the traverse gun speed to 240 mm/s. The thinner coatings present a suitable thickness to achieve

long-term stability of the implants and were used for biological characterization. It is worth indicating that this decision was taken since it is widely accepted that a high thickness can cause delamination and fragmentation of the coating before a good bond with the bone tissue is achieved (Ref 35, 36).

The microstructure and the distribution of the elements in the cross-section and the top surface of the coatings were observed by an SEM (JSM-5310, JEOL, Tokyo, Japan) equipped with energy-dispersive x-ray spectrometry (EDS). For the chemical analysis, an elemental mapping was done by EDS. The main element of this bioactive glass, silicon, was selected to identify the glass particles in the coating. To analyze the distribution of the glass particles, cross-sections of the coatings were prepared by cold mounting resin, ground with silicon carbide abrasive papers up to P4000 (grit size 5 μm), and polished with 1- μm diamond slurry. Cross-sections and surface coatings were gold-coated prior to the observation.

Crystallographic structure analysis of PEEK powder and PEEK 100% coating was performed by x-ray diffraction (XRD) using a diffractometer (X'Pert PRO MPD, PANalytical, Cambridge, UK).

Image analysis of the EDS micrographs was done to quantify the area percentage of glass material either incorporated into the composite coating or exposed to the media on the coating surface; for this purpose, ImageJ software was used. The analysis was applied to the SEM images taken from the surface and cross-section of the coatings (five images at a magnification of 200x for each sample). The stages of image processing were as follows: first, the acquisition of the image; second, the selection of the channel of interest (specific color channel corresponding to silicon); then the adjustment of the threshold level to eliminate noise and finally, the identification and quantification of the area. The authors know that the area percentage value measured and calculated by this method does not represent the actual content of 45S5 in the coating but an estimation of this value. However, because of the inertness of both materials, image analysis may provide a correlation between feedstock blend and coating compositions, and as a result, with the biological response of the coatings.

Bioactivity and Degradation Assessment

To evaluate the ability of the coatings to form an HCA layer, an *in vitro* test was performed following ISO 23317 (Implants for surgery - *In vitro* evaluation for the apatite-forming ability of implant materials). Samples were immersed, in the vertical position, in Hank's balanced salt solution (HBSS) (Sigma-Aldrich, Germany) in a thermostatic bath with agitation at 37 °C. The solution was

refreshed twice a week to avoid ionic saturation of the medium. The evaluation of the HCA formation was studied at different periods: 0, 3, 7, 14, and 21 days. Three samples of each coating type were immersed for each exposure time. After immersion, samples were rinsed with ultrapure water and dried for 24 h at room temperature.

The surface of the samples was observed using an SEM (JSM-5310) to evaluate the HCA layer's formation process at each period. For this observation, all the specimens were gold-coated to allow them to be conductive.

Furthermore, the formed layer was analyzed from the cross-sectional images of the samples immersed for 7 and 21 days. For this examination, the cross-sections were prepared as described previously. After being dried in a desiccator for 48 h, the samples were gold-coated and examined by SEM (JSM-5310). In addition, the composition of the formed layer after 21 days was analyzed by EDS on the cross-sections.

To assess the crystallization of the formed layer of HCA, crystallographic structure analysis of the samples immersed for 14 days in HBSS was performed by XRD.

A degradation study was performed to evaluate the glass dissolution of the different coatings. Following the specifications of ISO 10993-14 (Biological evaluation of medical devices - Part 14: Identification and quantification of degradation products from ceramics), the samples were immersed in a buffered solution consisting of Tris-HCl with pH adjusted to 7.4 ± 0.1 at 37 ± 1 °C for 120 h.

Three coated samples for each condition, 8×8 mm in size, were immersed in 50 mL of Tris-HCl solution for the test. The samples were weighted with a high-precision scale (CPA225D, Sartorius, Goettingen, Germany) before and after the test to determine the weight loss percentage due to degradation. After exposure, the samples were rinsed thrice with ultrapure water and dried overnight at 120 °C before being weighted. At the end of the test, pH was recorded using a universal pH meter (Hach, Spain). The silicon, calcium, and sodium concentrations were measured by inductively coupled plasma optical emission spectrometry (ICP-OES) (Optima 8300, PerkinElmer, Waltham, USA). Moreover, the samples' surfaces after degradation were observed by SEM.

Cell Culture Studies

Osteoblasts were seeded onto different coatings to study the ability of the samples to allow adhesion, growth, and proliferation of this cellular type. The tests were repeated in triplicate with different human osteoblast lines (obtained from knee trabecular bone after prosthesis replacement (Ref 37) in a passage from 3 to 6 to obtain reliable results. Three different biomaterials of each series were evaluated in each experiment, and controls of tissue culture plastic

(TCP) were also included. In order to avoid the inter-experiment variability, results were normalized to the TCP at three days within each experiment. Parc de Salut Mar Ethics Committee approved the study.

Before the cellular tests, samples were sterilized in ethanol 70% for three hours to avoid contamination during the test. After sterilization, samples were immersed in Dulbecco's modified Eagle's medium (DMEM) (Invitrogen, USA) supplemented with 10% fetal bovine serum for 24 h. This precondition step is necessary to avoid cell death caused by increased pH due to the rapid release of ions from the glass (Ref 38). A cell suspension was prepared and seeded at a 6.5×10^3 cells/sample density with supplemented DMEM onto the coated samples placed in a 48-well polystyrene plate. The incubation was done at 37 °C in a humidified atmosphere of 5% CO₂, changing the media every three days.

After 3, 7, and 14 days of incubation, cell proliferation was analyzed using an MTS assay (CellTiter 96® Aqueous One Solution Cell Proliferation, Promega, USA). This colorimetric test allows the quantification of viable cells based on the reduction of MTS tetrazolium by cells into a colored formazan product soluble in a cell culture medium. After each period, the medium was removed from the wells, and the samples were transferred to new wells. Then, the samples were incubated with 50 µl of MTS reagent and 250 µl of supplemented medium for 1 hour and a half. Afterward, the absorbance was recorded at 490 nm using a well plate reader (Infinite 200, Tecan, Männedorf, Switzerland).

The quantitative results from the MTS assay were analyzed using a one-way analysis of variance (ANOVA) followed by Tukey's post hoc test to determine differences among groups. Where $p < 0.05$ was considered to be statistically significant.

SEM (Phenom ProX) was used to analyze the attachment and morphology of the cells. Osteoblasts were seeded onto the coatings at the same density as for the MTS assay. After 24 h of incubation, the samples were washed twice with phosphate-buffered saline (PBS) buffer (pH 7.4) to remove non-bounded cells. The remaining cells were fixed with 2.5% glutaraldehyde in PBS for three hours. After that step, the samples were rinsed twice with PBS. The dehydration of the cells was performed with ethanol baths of 15 minutes each, increasing the ethanol concentration as follows 50, 65, 70, 80, 90, 95, and 100%, respectively. Finally, the samples were dried using a critical point dryer (CPD) (K850, Emitech, Lewes, UK) and carbon-coated for the SEM observation using a high-vacuum carbon evaporator (K950X, Emitech, Lewes, UK).

Results and Discussion

Powder and Coating Characterization

In CGS, the particle size of the powder has a significant influence on the coating achieved. Xu et al. (Ref 39) studied cold spray deposition of thermoplastic coatings at different particle sizes with the same air pressure. They found that higher final velocities and higher mass deposits were achieved for the smaller particles, which experienced increased acceleration. For this reason, commercial powders were sieved to work with appropriate particle size and then characterized to corroborate the correct processing of the feedstock materials.

The SEM analysis performed on the powders allowed us to establish their morphology and size differences, as shown in Fig. 1. Specifically, the 45S5 glass particles are dense and irregular, with corners and sharp edges, a typical result for crushed particles after the melt-quenching process. In addition, it is here observed that the particles are quite similar in size to each other. On the contrary, PEEK powder comprises small, aggregated particles that form more rounded and less compact agglomerated particles than glass ones. In general, it is appreciated by SEM inspection that the PEEK particles are smaller and have a more significant variation in particle size than glass particles.

The particle size distribution of both powders measured by laser diffraction can be observed in Fig. 1. The glass particles exhibit a narrow distribution, achieved with the sieving process with the following characteristic values related to size distribution: $d_{10} = 28.1 \mu\text{m}$, $d_{50} = 41.1 \mu\text{m}$, $d_{90} = 53.2 \mu\text{m}$. Both powders were sieved with a 40- μm mesh, and the fraction below this mesh was selected. Even though glass particles above this size are detected, which may be associated with the irregular morphology of these particles that can pass through the mesh on their thinnest side during the sieving process. By contrast, the PEEK powder exhibits a slightly bimodal nature, and the size distribution of the sieved powder is characterized by $d_{10} = 10.2 \mu\text{m}$, $d_{50} = 21.2 \mu\text{m}$, and $d_{90} = 37.6 \mu\text{m}$. The values obtained with this technique are consistent with the observations by microscopy.

Blends of the sieved 45S5 and PEEK powders with the compositions listed in Table 1 were sprayed by LPCGS using the spraying parameters detailed in the Material and Methods section. The microstructure of the deposited coatings in the cross-section is shown in Fig. 2. The observation reveals two different regions. The PEEK particles form a dense and continuous matrix (the dark gray region in Fig. 2). In contrast, the glass particles (the light gray in Fig. 2) are embedded in the polymeric matrix, suggesting that the PEEK particles reach a temperature above its glass transition temperature and therefore have

Fig. 1 Particle size distribution in volume and SEM micrographs of the bioactive glass (A) and PEEK (B) powders

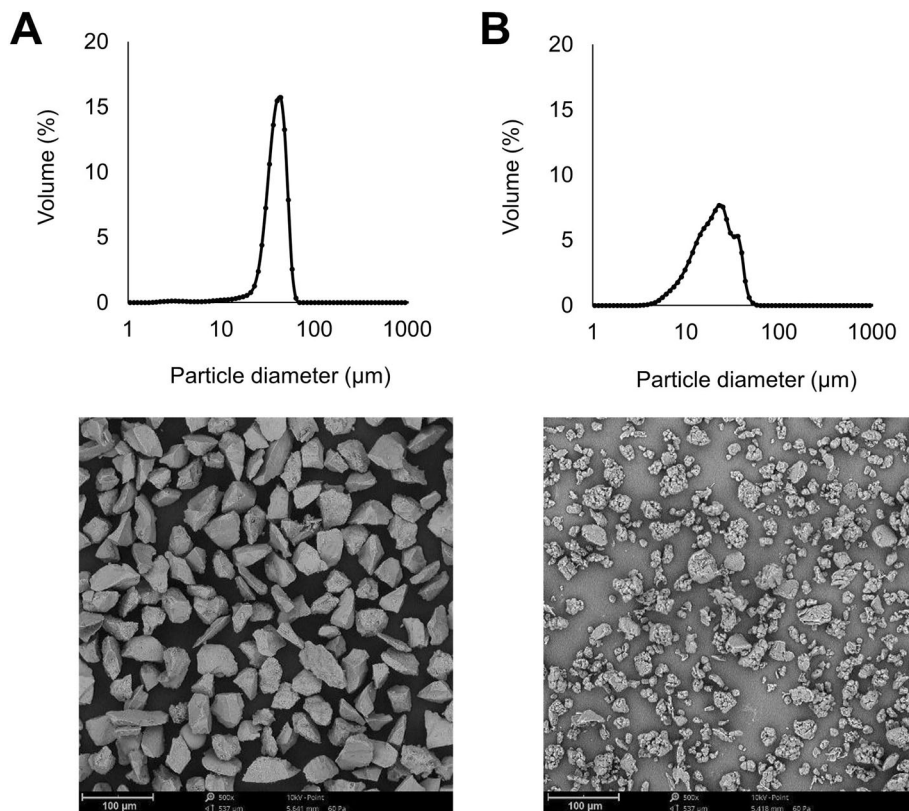
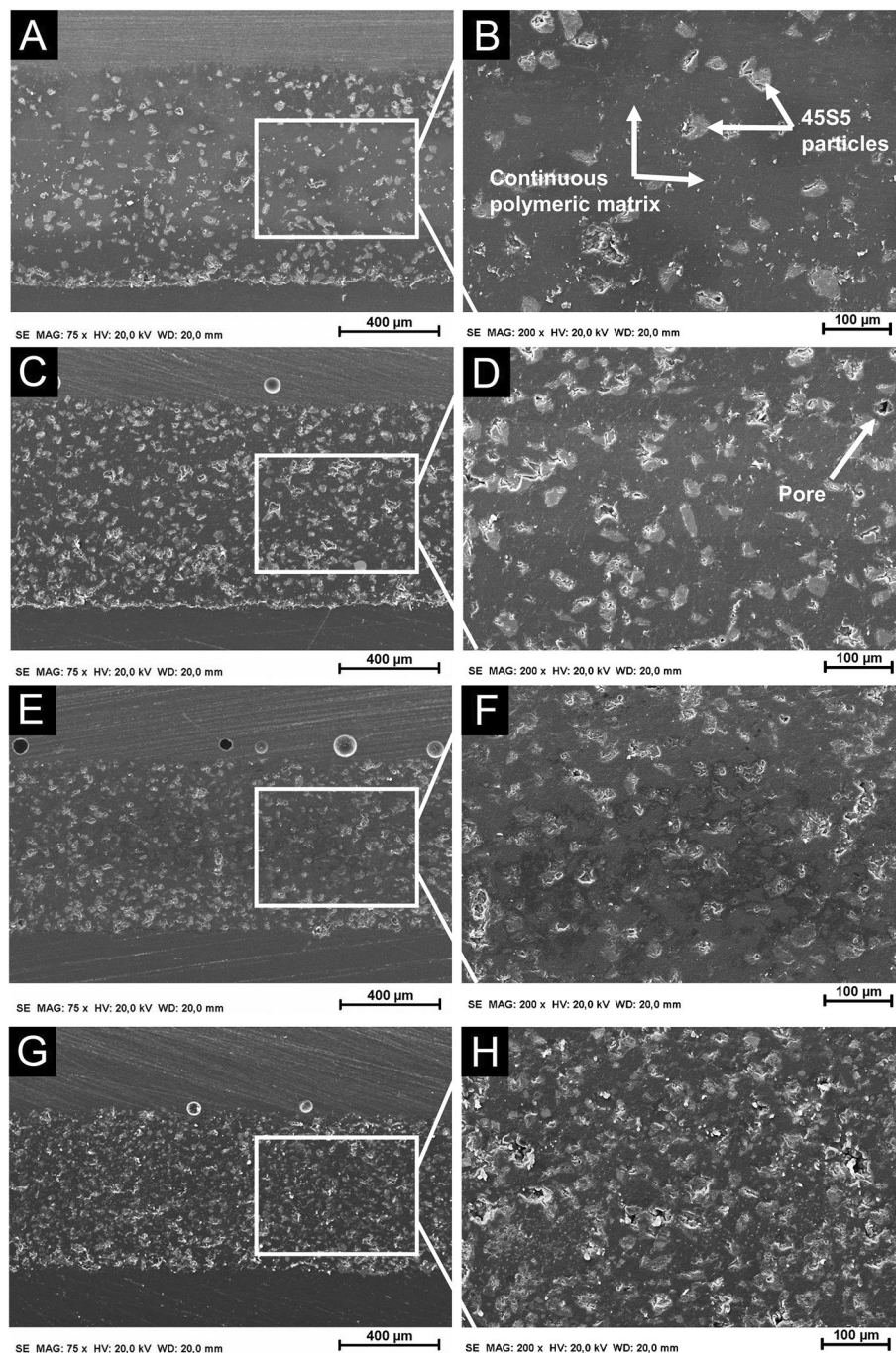


Fig. 2 Cross-sectional SEM micrographs: (A) and (B) 45S5 10%, (C) and (D) 45S5 25%, (E) and (F) 45S5 35%, (G) and (H) 45S5 50%



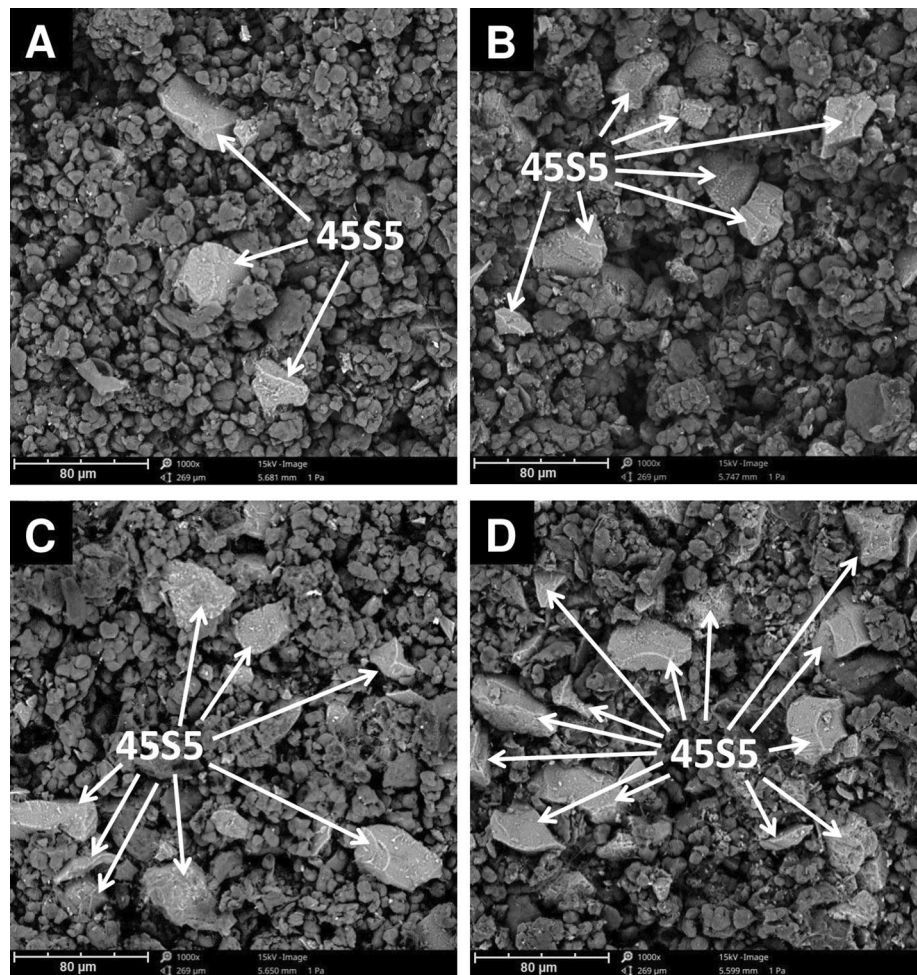
been plastically deformed during the process, while the bioactive particles are perfectly surrounded and retained by the polymeric matrix, maintaining their initial morphology, which indicates that glass particles have not been plastically deformed during the spraying process. Moreover, some porosity between particles can be observed in the coatings with more glass.

The top surface of the sprayed coatings containing glass is shown in Fig. 3. It is possible to observe how the glass particles are surrounded by polymeric particles, and more

glass particles are observed on top of the coatings with higher glass content in the blend. In the upper layer of the coatings, the particles reached the substrate with slight deformation, since in CGS, the deformation of the particles in the coating is mainly achieved when they are impacted by the following particles deposited on them.

The analysis of the cross-sections and the surfaces corroborates the success of producing a composite coating, which includes bioactive glass particles embedded in a polymeric matrix. Furthermore, the deposition of the

Fig. 3 Top surface SEM micrographs: (A) 45S5 10%, (B) 45S5 25%, (C) 45S5 35% and (D) 45S5 50%



coatings has been achieved without altering the composition of the bioactive particles using CGS since the particles have maintained their morphology and have been kept below their glass transition temperature (550 °C) all over the coating formation.

During the spraying process with LPCGS, the gas temperature was set at a maximum of 350 °C. However, due to the process's speed, we can consider that the sprayed blends were in contact with the hot flow of gas only for a brief period. Furthermore, polymeric and ceramic materials are known to have low thermal conductivity. Under these conditions, it was expected that the particles did not reach the temperature of the gas. When the PEEK particles impinge onto the substrate, it is suggested that particles should be between glass transition and melting temperature. As it is well known, the glass transition temperature of PEEK starts at 143 °C, the melting is achieved at 343 °C, and decomposition occurs at 575 °C (Ref 40, 41). In this temperature range, the thermoplastics can be deformed plastically and explain the dense polymeric matrix observed in the cross-sections, in which the separation between PEEK particles is not appreciated. On the other

hand, the glass transition temperature of the 45S5 occurs at 550 °C, and melting is evidenced at 1070 °C (Ref 42, 43). Consequently, to undergo plastic deformation, the glass particles require higher temperatures than those reached during the process.

XRD patterns of the PEEK powder before spraying and the PEEK 100% coating are displayed in Fig. 4. The crystallographic structure analysis was done to determine whether the crystalline phase of PEEK changed after spraying. Both patterns exhibit broad peaks, as expected for semicrystalline polymers. The identified peaks coincide with the PEEK (Reference code: 00-053-1992), and the intensity is very similar for both the powder and the coating. The results suggest that the coating manufacturing process has kept the crystallinity of the PEEK polymer.

For a good bioactive response of the coating, the glass particles must be well distributed throughout the coating, especially these must be present on the surface of the coating that, in the end, it is the part of the component that will be in direct contact with body fluids.

Image analysis was performed on the top surface and cross-section of the different coatings to quantify the glass

Fig. 4 X-ray spectra of PEEK powder and as-sprayed PEEK 100% coating

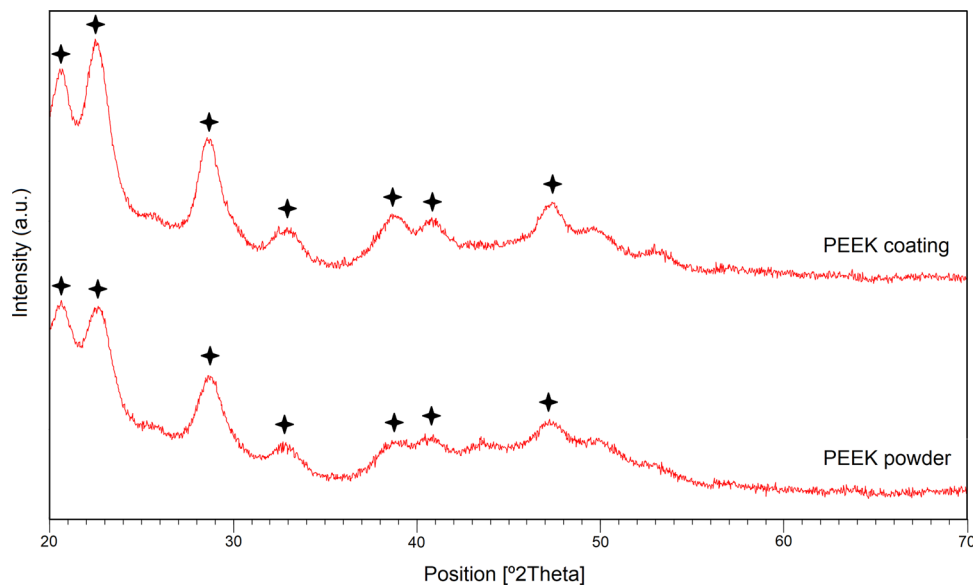
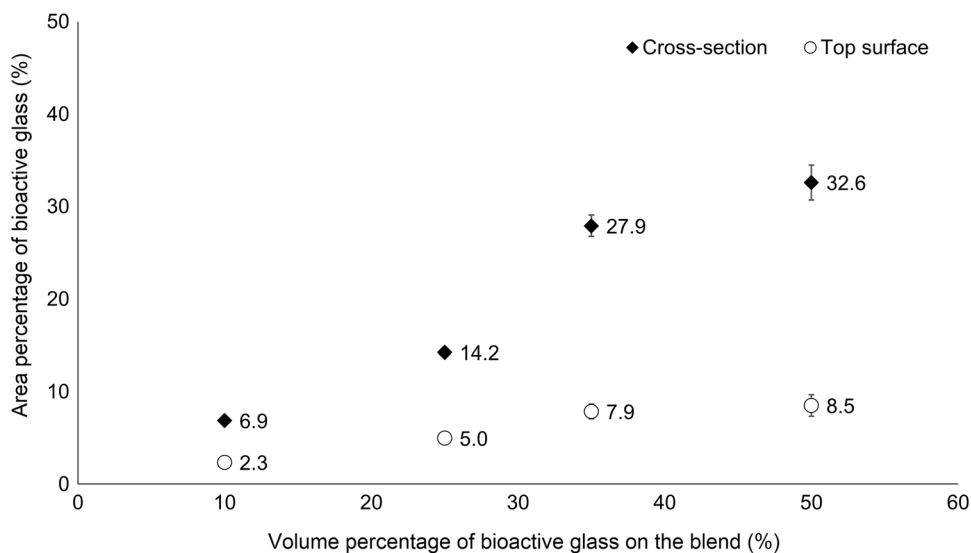


Fig. 5 Area percentage of bioactive glass quantified vs. volume percentage of bioactive glass on the blend



particles retained in the coatings. It was done following the procedure described in the Material and Methods section. This method made it possible to compare the amount of bioactive glass particles retained with the blend composition sprayed. Thus, the percentage of the area corresponding to glass material in the coating cross-section and top surface is represented versus the volumetric percentage of glass on the sprayed blends in Fig. 5. It should be noted that the values shown cannot be compared with the volumetric percentages of the blends.

For both the cross-sections and the top surfaces, a gradual increase in the glass area can be observed related to the amount of glass in the sprayed blends up to a glass content of 25%. In addition, from 35% glass in the blend, the increase in glass retained in the cross-section and on the

surface is less significant. For the coatings with the highest glass content, the glass particles are rebounding when they impinge onto other glass particles that are already part of the coating, having a lower ability to be retained by the polymeric matrix but generating a kind of erosion on top of the coating. The results corroborate that the glass particles are present inside the coating and on the surface. These composite coatings could promote the bioactive response of coated PEEK because of the presence of bioactive particles on their surface.

In Vitro Bioactivity Study—Ability to Form Apatite

The presence of glass in the coatings is expected to provide bioactive capacity to the samples since the ionic dissolution

of glass stimulates the formation of the HCA, which promotes the osteointegration between bone and implant.

The formation of the apatite layer follows a sequence of rapid reactions described by Hench: (i) ion exchange between glass and solution, (ii) formation of silanols at the glass solution interface, (iii) formation of a silica-gel layer by condensation and re-polymerization of silanols, (iv) formation of a CaO-P₂O₅-rich layer by incorporation of calcium and phosphate from solution, and (v) crystallization of the amorphous CaO-P₂O₅-rich layer to form crystalline HCA layer (Ref 44, 45).

Due to the great importance of this HCA layer in implant osteointegration, all the composite coatings were immersed in an HBSS solution for 21 days, and the surface of the coatings was periodically evaluated to analyze the formation of the HCA layer. SEM micrographs of the PEEK 100% coating (Fig. 6) after 14 days of immersion in HBSS revealed that PEEK coatings could not form an HCA layer as expected if we consider that this material is not bioactive. By contrast, it can be observed that the key role that 45S5 has is a bioactive coating component even at low content; all the coatings containing glass particles can form the HCA layer. The coatings with a glass content higher than 10% followed similar behavior regarding forming the HCA layer. In them, the incorporation of 45S5 glass promoted quicker development of the HCA layer

compared to 45S5 10% coating. Furthermore, it is possible to appreciate the higher presence of small apatite spheres at 3 days. In particular, apatite deposits have begun forming on the top of glass particles. On the contrary, in the 45S5 10% coatings, small apatite spheres were identified in the early stages of the experiment (at 3 days of immersion), which grew and formed aggregated deposits after 7 days of immersion, until finally entirely covered the surface of the coating by a continuous HCA layer after two weeks of the test. At 21 days of exposure, the HCA layers of all coatings with glass content continued growing. However, the micrographs corresponding to that period are not shown in Fig. 6 due to their similarity with the previous period.

These images allow us to validate the bioactive capacity of the coatings with glass content. The results suggest that coatings obtained by cold-spraying 45S5-PEEK blends with at least 25% of glass promote a fast HCA layer growth, which can lead to a successful implant osteointegration. The coatings obtained with the 45S5 10% blend also present bioactivity but with a considerable decrease in the kinetic of HCA formation concerning the other coatings. As expected, PEEK 100% coatings could not form an HCA layer after 21 days in the solution.

The few bioactive glass particles found on the top surface of the coatings (Fig. 5) have been shown to promote the formation of the HCA layer. However, the coatings

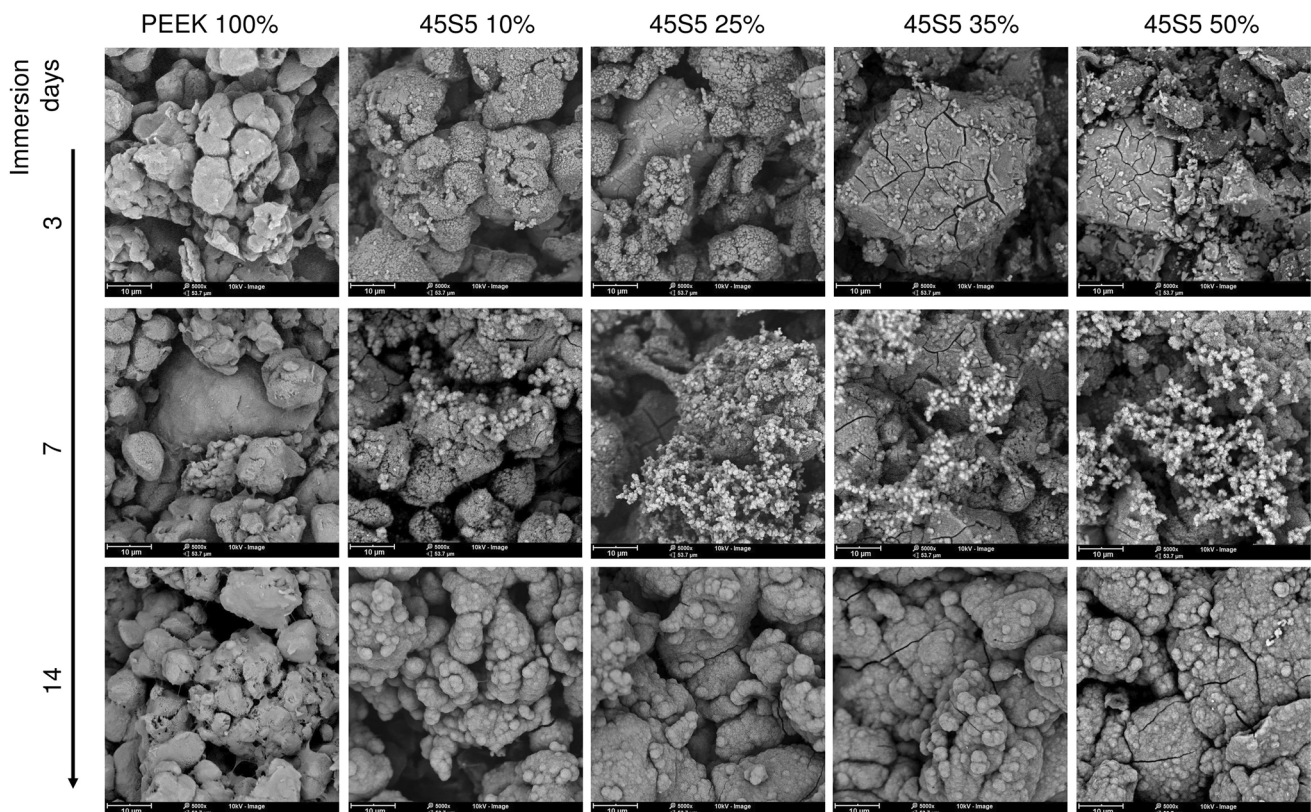


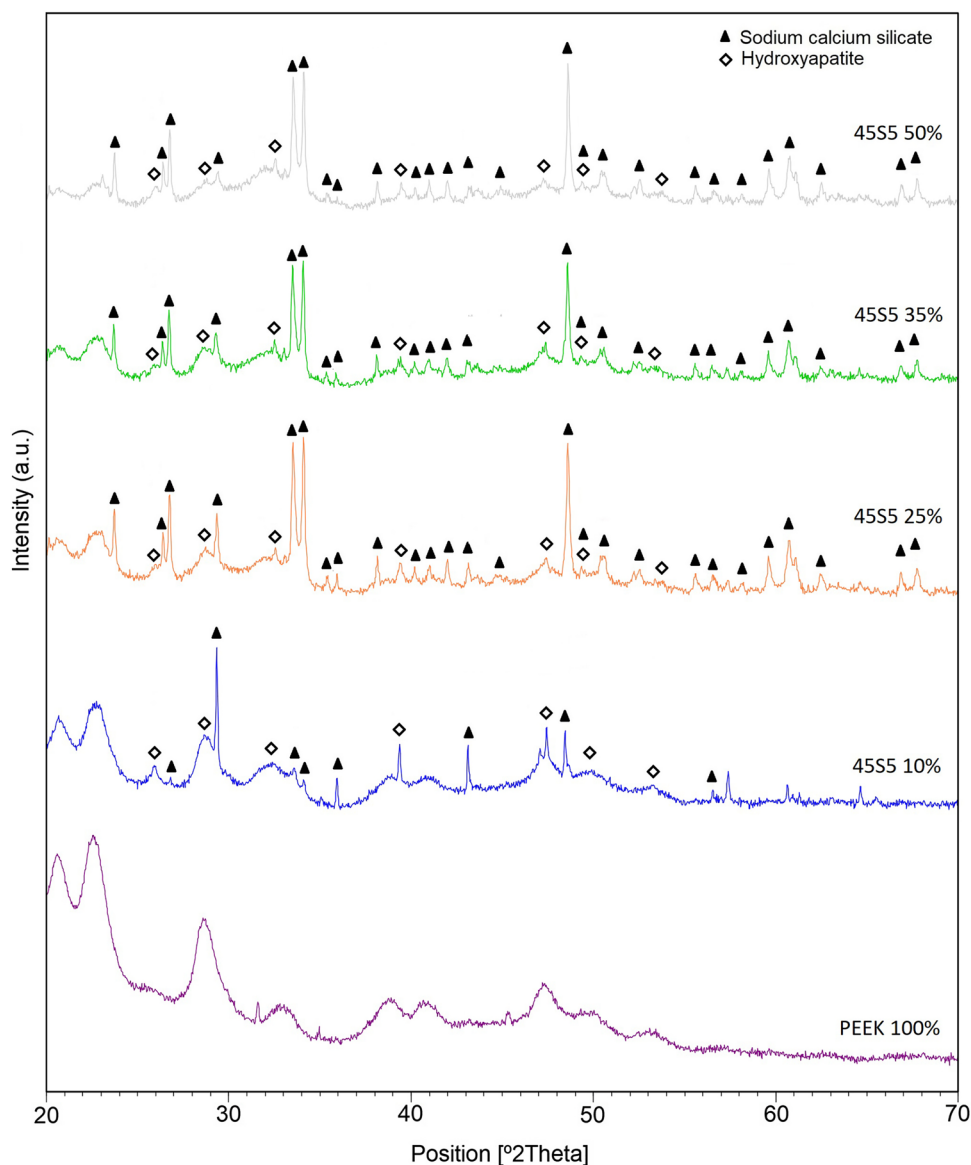
Fig. 6 SEM images of the surface of the samples after soaking in HBSS for different times: after 3, 7, and 14 days

need 14 days of immersion to be fully covered by a bone-like apatite layer. In comparison, in other studies with more presence of bioactive materials on the top surface, the HCA layer covers the coatings completely in shorter periods: Ur Rehman et al. (Ref 46) at 3 days, Garrido et al. (Ref 24) at 6 days or Yu et al. (Ref 47) at 7 days.

X-ray diffraction analysis was used to confirm the formation of HCA layers on the surface of the coatings immersed for two weeks in HBSS. XRD patterns of the rinsed and dried coatings after these 14 days are illustrated in Fig. 7. The pattern of the pure PEEK coating revealed broad peaks corresponding to the crystalline phase of the PEEK polymer. The absence of peaks related to the formation of the HCA layer corroborates the lack of bioactivity of the inert coating, according to the SEM images of Fig. 6, where no change in the surface of these coatings can

be detected. In the patterns of the coatings containing glass, the detected peaks are consistent with sodium calcium silicate ($\text{Na}_6\text{Ca}_3\text{Si}_6\text{O}_{18}$; code: 01-079-1089) and hydroxyapatite ($\text{Ca}_5(\text{PO}_4)_3(\text{OH})$; code: 00-001-1008), related to the presence of bioactive glass particles and the HCA layer formation. The sodium calcium silicate phase is not related to the *in vitro* test. It is the result of the self-crystallization that 45S5 glass undergoes at room temperature and atmospheric pressure, as reported in a published study (Ref 48). The intensity of the peaks corresponding to the HCA layer is similar for the different composite coatings. Besides, it is possible to appreciate a trend of lower intensity in the peaks associated with PEEK as the amount of glass in the coating increases due to the lower amount of PEEK in these coatings. Considering the hydroxyapatite peaks, the XRD results suggest that the growth kinetics of the apatite

Fig. 7 X-ray spectra acquired on the samples after immersion in HBSS for 14 days.



layer was not affected by the increase in glass in the coating.

The cross-section of the formed layer of HCA after 7 and 21 days of exposure can be observed in Fig. 8. After one week, a thin layer (light gray) was formed on the different coatings. However, this HCA layer is not continuous along all the coating, particularly in the 45S5 10%; some parts are behavior without apatite deposition. These results agree with the SEM images observation in Fig. 6 at 7 days, where 45S5 10% coatings showed a slower rate of apatite formation than the other glass coatings. At three weeks, the HCA layer has grown for all the samples, becoming continuous throughout all the surface coating and reaching a thickness between 2 and 4 μm. In addition, after 21 days of exposure, the absence of glass particles (light gray) in the coatings could be observed. It corroborates the process described in the literature, in which the formation of the apatite layer is related to the degradation of bioactive glass. In order to corroborate the composition of the formed layer of HCA, chemical analyses were carried out, and the atomic concentration measured is detailed in Table 2. The chemical analysis confirms the presence of a layer rich in apatite, and in particular, the Ca/P ratio (atomic) after three weeks of test reveals values near the crystalline hydroxyapatite (1.67) (Ref 49). The ratios obtained are coherent with the values reported by other authors (Ref 50, 51).

Degradation Study

The degradation rate and the ion release of bioactive glasses can strongly affect the biocompatibility of the coatings. Furthermore, the capacity of bioactive glass particles to be replaced by bone is tightly linked to their

dissolution. For this reason, a degradation study of the developed coatings can provide valuable data on their biological capabilities.

The weight loss associated with the degradation of the glass retained on the coatings was studied in the degradation test. The coated samples were immersed for 120 h in Tris–HCl solution, and the percentages of weight loss of the samples and the pH values measured after the test are illustrated in Fig. 9.

Incorporating bioactive glass in the coatings resulted in a remarkable increase in degradation compared to the pure PEEK coating, which is non-degradable in physiological fluids. The increased weight loss observed can be connected with the area percentage of bioactive glass quantified on the surface of the coatings shown in Fig. 5. Remarkably, the two coatings with more glass content (45S5 35% and 50%) achieved the same weight loss values (1.00 and 0.99%), suggesting that the glass found on the surface was not significantly different in both cases. Furthermore, the ions released from the glass particles of the coatings cause an increase in the pH solution, proportional also to the amount of glass in contact with the solution.

Table 2 EDS scan onto the formed layer of HCA after test in HBSS for 21 days

	Atomic concentration			
	45S5 10%	45S5 25%	45S5 35%	45S5 50%
Oxygen%	69.6	66.4	70.2	69.0
Calcium%	19.2	21.4	19.0	19.8
Phosphorus%	11.2	12.2	10.8	11.2
Ca/P ratio	1.71	1.75	1.76	1.77

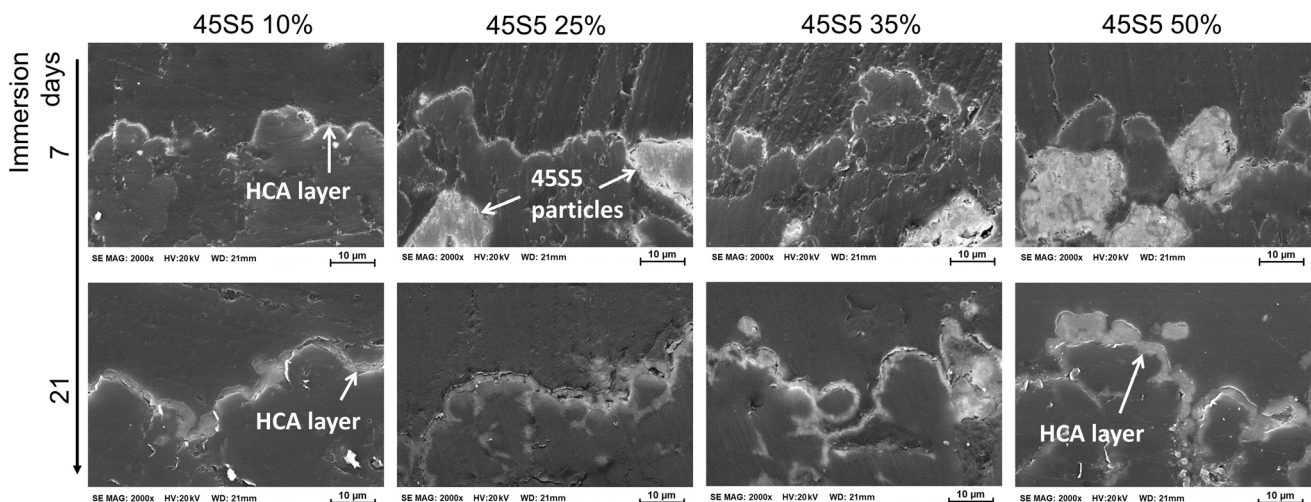


Fig. 8 Cross-section micrographs showing the HCA layer after 7 and 21 days of immersion in HBSS

Fig. 9 Weight loss rate of coated samples after soaking in Tris-HCl solution (bars) and pH value recorded after the test (×)

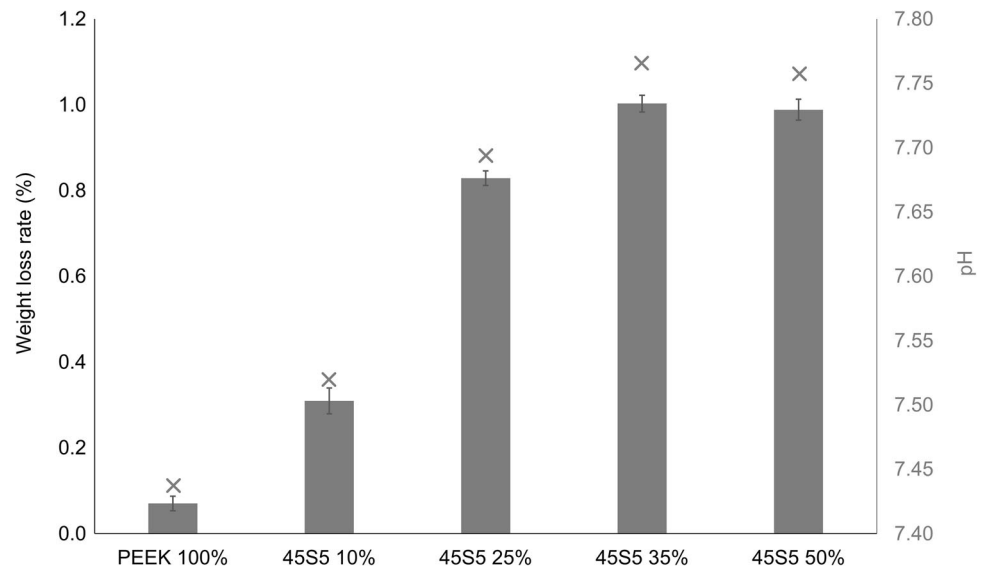
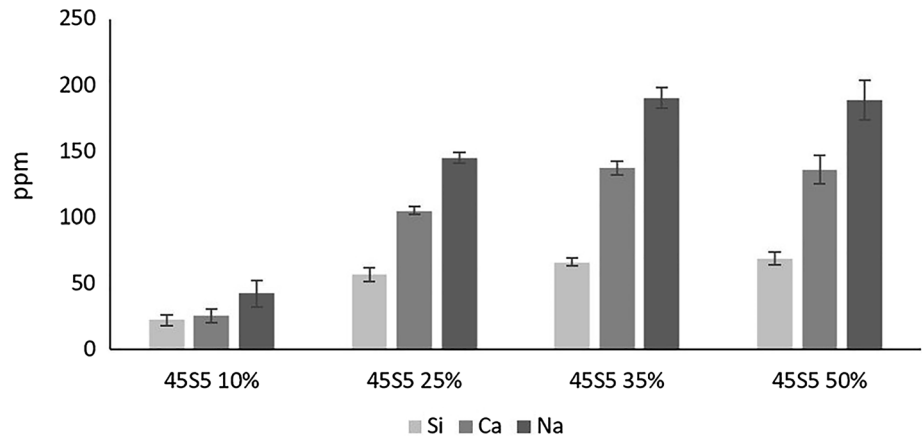


Fig. 10 Ion release into Tris-HCl solution after immersion of samples for 120 h



The dissolution products of the bioactive glass of the coatings promote the formation of the HCA layer, as evidenced in the cross-sections after 21 days of immersion in HBSS, where the glass particles near the surface were dissolved (Fig. 8). After the degradation test, the chemical contents of the solutions were measured using ICP-OES. The concentration of elements released (silicon, calcium, and sodium) at 5 days is shown in Fig. 10. The ions corresponding to the dissolution of the glass were detected, which are associated with the loss of weight of the coatings studied. These results are consistent with the lower bioactive capacity observed on the 45S5 10% coatings, as discussed previously in section 3.2.

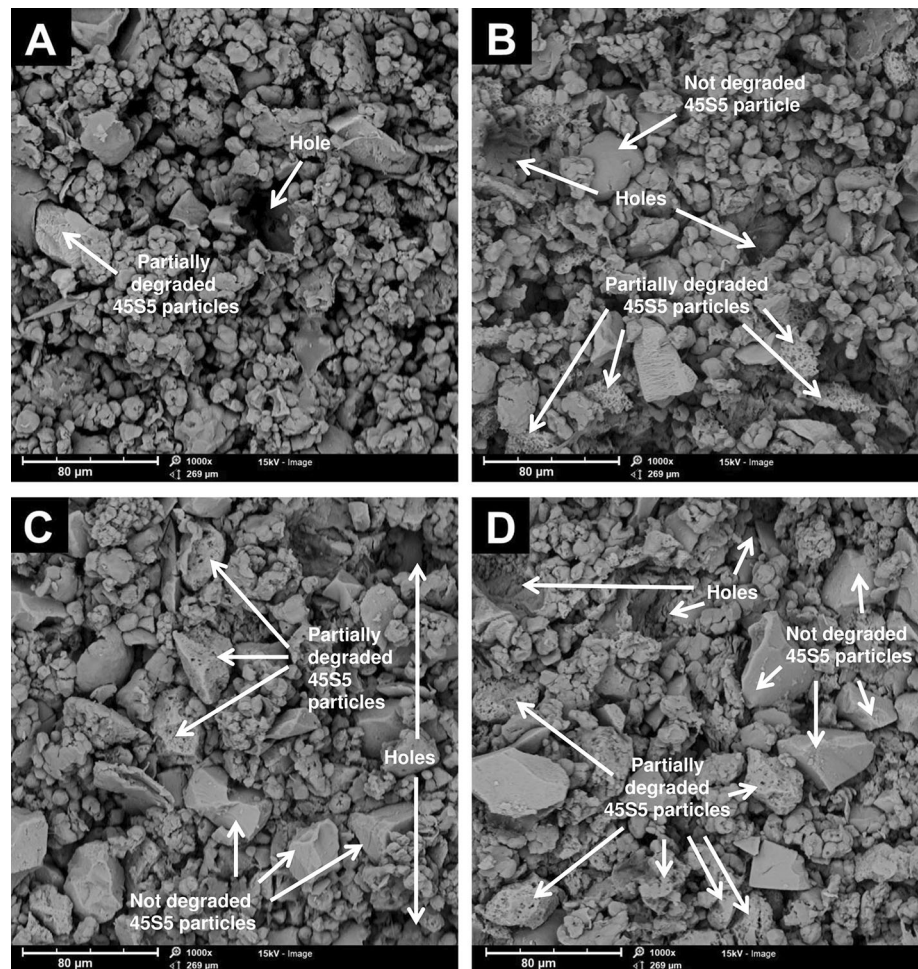
According to Hench (Ref 52), the first step in bioactive glass dissolution is the release of alkali modifier cations (Na + in 45S5), consistent with our results, where sodium ions are the most released, followed by calcium ions. Both are the modifying elements of the network, consequently, the most susceptible to being released. In addition, the

release of network-forming elements (silicon and phosphorus) was lower. Only silicon ions were detected in the solution due to the high contribution of silicon oxide (45.0 wt.%) on this specific glass composition. Phosphorus was not detected due to the low content in the original glass (6.0% wt.%).

This ion exchange process caused by immersion in HBSS of glass particles increases the solution's pH and the glass particles' dissolution. The results from this analysis perfectly match the weight loss, and pH values discussed previously and validate the analysis of the bioactive response of the coatings.

Figure 11 shows the top surface of the coatings containing glass after degradation. Some glass particles are partially degraded, mainly on the coatings with more glass content. Other glass particles have not started to degrade, and there are also some holes at the surface of the coatings. However, these holes can be related to glass particles that

Fig. 11 Top surface SEM micrographs after degradation: (A) 45S5 10%, (B) 45S5 25%, (C) 45S5 35% and (D) 45S5 50%



were entirely degraded or can be generated during the spraying, as observed in Fig. 3.

By combining the results from the different techniques employed to study the bioactivity and degradation of the coatings, we could conclude that the presence of glass in the coatings is vital to acquiring bioactive behavior. In comparison, the coatings with more glass on the blends provide comparable bioactive capacity, due to the more similar amount of glass retained in the sprayed coatings, particularly on the surface. Moreover, the bioactive capacity of the 45S5 10% coatings is considerably lower than the other ones.

Cell Culture Study

The integrity of the coatings obtained by LPCGS is related to the glass content in the blend. As the amount of glass increases, erosion begins to occur, and the ability of the polymeric matrix to retain the glass particles decreases. In addition, the results obtained in the apatite layer formation and degradation tests are correlated with the amount of

glass exposed on the surface, where no significant differences were obtained for the coatings with higher glass content (45S5 35 and 45S5 50%). Therefore, cell assays were performed only on the following coatings: PEEK 100, 45S5 10, 25, and 35%. TCP was also included as a positive control.

PEEK is a biomaterial that does not favor cell adhesion due to its high hydrophobicity (Ref 53). Compared to other materials such as titanium, tantalum, or even bioactive glasses, the cellular response of PEEK is low, and strategies to induce positive cellular responses and osteointegration are required (Ref 2, 7, 54). The results of adhesion and proliferation of osteoblasts on the studied coatings at different periods are plotted in Fig. 12. Similar cellular activity was observed between the different coatings for short- and long-term periods. Other studies have already reported that, in short-term periods, no differences were observed in cellular response between pure PEEK samples and PEEK/bioactive-ceramic samples (Ref 32, 55–57). However, the ternary biocomposite developed by Deng et al. (Ref 57) revealed

Fig. 12 MTS activity analysis for human osteoblasts after incubation onto PEEK 100%, 45S5 10%, 45S5 25%, and 45S5 35% at 3, 7, and 14 days. ($n = 9$; p -values < 0.01).

*Significantly more cells in the indicated group compared to the other groups at the same time point. †Significantly fewer cells than 45S5 25% and 45S5 35% at the same time point. #Significantly fewer cells than 45S5 35% at the same time point

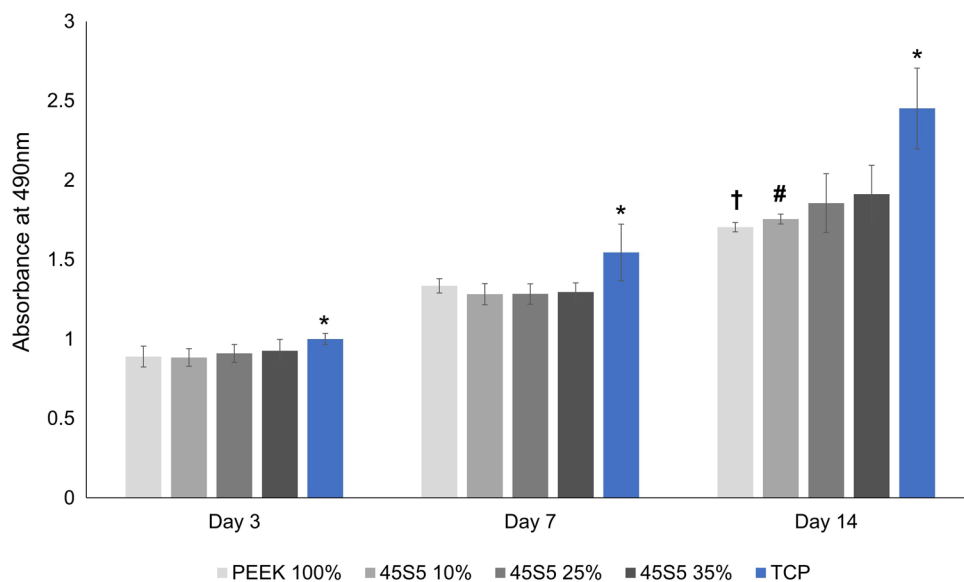
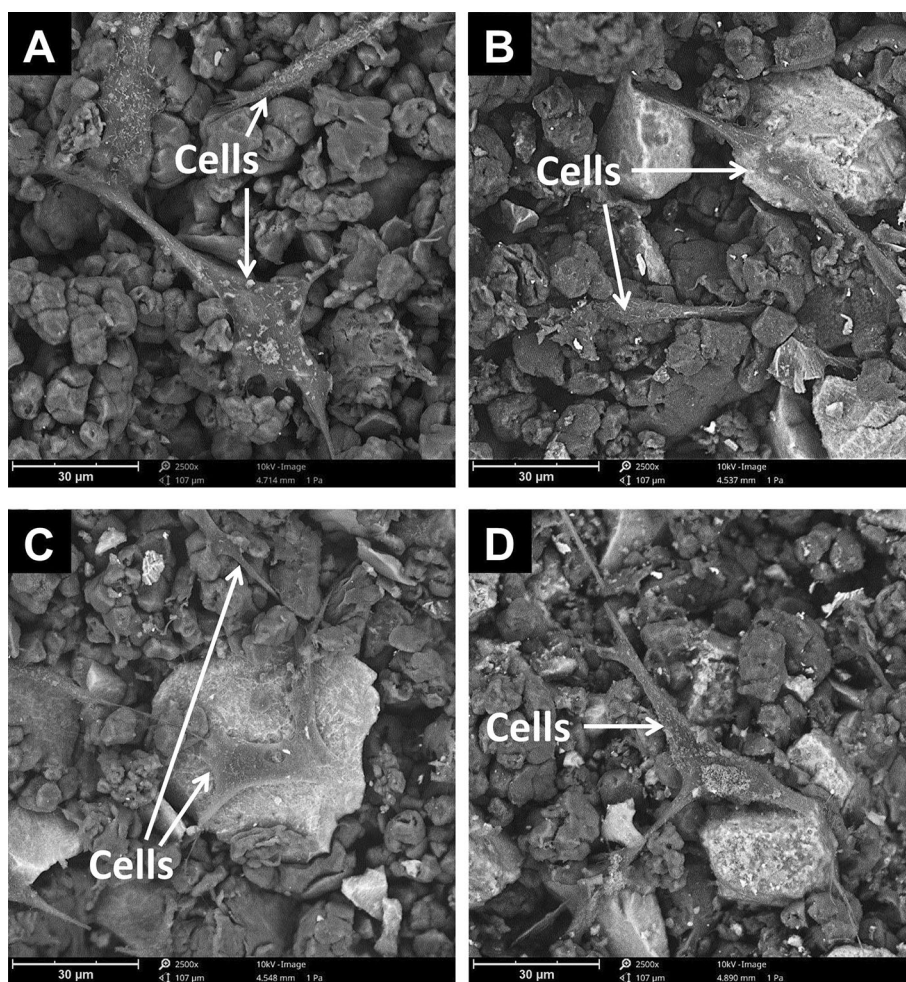


Fig. 13 SEM observation of osteoblasts after 24-h incubation ($\times 1500$). (A) PEEK 100%, (B) 45S5 10%, (C) 45S5 25%, and (D) 45S5 35%



an enhancement in cellular response at 7 days. According to the results of our study, there are no significant differences in cell proliferation caused by the presence of

glass in the coatings; possibly, the amount of glass on the surface is not enough to promote the expected improvement.

The morphological aspect of cells onto the coating surfaces was observed by SEM; micrographs after 24 hours of culture are shown in Fig. 13. The darkest particles correspond to PEEK, while the lighter ones are glass particles. In general, osteoblasts seeded onto the coatings with and without glass content showed the same morphology; the cells adhered to the coatings with long filopodia, showing a typical cell morphology for this type of cell. From these images, it can be concluded that cells can adhere to the top of both materials that form the coatings (PEEK and 45S5). The roughness of the different coatings is practically the same for all cases (values of Ra between 7.6 and 8.6 μm); therefore, this factor has not affected the cell culture results.

Conclusions

In this work, we have produced 45S5/PEEK composite coatings with enhanced biological properties using LPCGS. The ratio of glass in the sprayed blends was studied, by analyzing the quality of the coatings in terms of microstructure and the *in vitro* response, with results that show an improvement in the properties of the coatings due to the presence of glass. However, interesting differences among coatings were observed.

The produced coatings were composed of a dense polymeric matrix, where the glass particles were embedded without being altered during the deposition process. The microstructure analysis revealed that the polymeric matrix's capacity to retain glass is limited since increasing the amount of glass in the blends allows a maximum of glass incorporation for 35% of glass content.

The amount of glass on the surface is a crucial aspect of the bioactive behavior of composite coatings, as was demonstrated by the studies of the HCA layer formation and the degradation of the coatings. After three weeks of immersion, a continuous HCA layer could be seen in all the glass coatings, with a thickness between 2 and 4 μm . In particular, the formation of the HCA layer occurs at a similar rate for the coatings with 25, 35, and 50% of glass content in the blends, while coatings containing only 10% of glass in the blend showed slower kinetic reaction for HCA layer formation. In addition, the degradation rate of the different composite coatings was proven to be mainly related to the glass content on its surface, with an increase proportional to the identified glass area on the surface but reaching a top at 35% of glass in the blend. The bioactivity results were also supported by the weight loss, the ions release, and the pH values after the 120-h immersion in Tris–HCl solution.

Cellular *in vitro* studies showed that human osteoblasts could adhere and proliferate on the evaluated surfaces, with

similar cell proliferation for the different coatings evaluated. After 24 h of culture, osteoblasts were attached to the different materials forming the coatings.

Funding Open Access funding provided thanks to the CRUE-CSIC agreement with Springer Nature. This work was supported by the Spanish Government (MCIN/AEI/ <https://doi.org/10.13039/501100011033>) through grant MAT2016-76928-C2-1-R, Generalitat de Catalunya (SGR-1777) and the Centro de Investigación Biomédica en Red de Fragilidad y Envejecimiento Saludable-CIBERFES (CB16/10/00245) from Instituto de Salud Carlos III, and FEDER funds.

Open Access This article is licensed under a Creative Commons Attribution 4.0 International License, which permits use, sharing, adaptation, distribution and reproduction in any medium or format, as long as you give appropriate credit to the original author(s) and the source, provide a link to the Creative Commons licence, and indicate if changes were made. The images or other third party material in this article are included in the article's Creative Commons licence, unless indicated otherwise in a credit line to the material. If material is not included in the article's Creative Commons licence and your intended use is not permitted by statutory regulation or exceeds the permitted use, you will need to obtain permission directly from the copyright holder. To view a copy of this licence, visit <http://creativecommons.org/licenses/by/4.0/>.

References

1. P. Scolozzi, A. Martinez, and B. Jaques, Complex Orbito-Fronto-Temporal Reconstruction Using Computer-Designed PEEK Implant, *J. Craniofac. Surg.*, 2007, **18**(1), p 224–228.
2. S. Sarfraz, P.-H. Mäntynen, M. Laurila, S. Rossi, J. Leikola, M. Kaakinen, J. Suojanen, and J. Reunanen, Comparison of Titanium and PEEK Medical Plastic Implant Materials for Their Bacterial Biofilm Formation Properties, *Polym. Basel Switzerland*, 2022, **14**(18), p 3862.
3. J. Graham and J. Peck, (2012) FDA Regulation of Polyaryletheretherketone Implants, *PEEK Biomaterials Handbook*, S. Kurtz, Ed., 1st ed., William Andrew, 277–292.
4. L. de Ruitter, K. Rankin, M. Browne, A. Briscoe, D. Janssen, and N. Verdonshot, Decreased Stress Shielding with a PEEK Femoral Total Knee Prosthesis Measured in Validated Computational Models, *J. Biomech.*, 2021, **118**, 110270. <https://doi.org/10.1016/j.jbiomech.2021.110270>
5. Y.G. Koh, J.A. Lee, and K.T. Kang, Prediction of Wear on Tibial Inserts Made of UHMWPE PEEK and CFR-PEEK in Total Knee Arthroplasty Using Finite-Element Analysis, *Lubricants*, 2019, **7**(4), p 30. <https://doi.org/10.3390/lubricants7040030>
6. S. Verma, N. Sharma, S. Kango, and S. Sharma, Developments of PEEK (Polyetheretherketone) as a Biomedical Material: A Focused Review, *European Polym. J.*, 2021, **147**, p 110295. <https://doi.org/10.1016/j.eurpolymj.2021.110295>
7. S. Najeeb, Z.K. Bds, S.Z. Bds, and M.S.Z. Bds, Bioactivity and Osseointegration of PEEK Are Inferior to Those of Titanium: A Systematic Review, *J. Oral Implantol.*, 2016, **42**(6), p 512–516.
8. D. Almasi, N. Iqbal, M. Sadeghi, I. Sudin, MR Abdul Kadir, and T. Kamarul, Preparation Methods for Improving PEEK's Bioactivity for Orthopedic and Dental Application: A Review, *Int. J. Biomater.*, BD Ratner, AS Hoffman, FJ Schoen, and J Lemons Eds, 2nd ed, Hindawi Publishing Corporation, (2016), **2016**, 1–12

9. L.L. Hench and H.A. Paschall, Direct Chemical Bond of Bioactive Glass-ceramic Materials to Bone and Muscle, *J. Biomed. Mater. Res.*, 1973, **7**(3), p 25-42.
10. J.R. Jones, D.S. Brauer, L. Hupa, and D.C. Greenspan, Bioglass and Bioactive Glasses and Their Impact on Healthcare, *Int. J. Appl. Glas. Sci.*, 2016, **7**(4), p 423-434.
11. D.S. Brauer, Bioactive glasses—structure and properties, *Ange wandte Chemie Int. Edit.*, 2015, **54**(14), p 4160-4181.
12. C. Gabbi, A. Cacchioli, B. Locardi, and E. Guadagnino, Bioactive Glass Coating: Physicochemical Aspects and Biological Findings, *Biomaterials*, 1995, **16**(7), p 515-520. [https://doi.org/10.1016/0142-9612\(95\)91123-G](https://doi.org/10.1016/0142-9612(95)91123-G)
13. N.C. Lindfors, P. Hyvönen, M. Nyssönen, M. Kirjavainen, J. Kankare, E. Gullichsen, and J. Salo, Bioactive Glass S53P4 as Bone Graft Substitute in Treatment of Osteomyelitis, *Bone*, 2010, **47**(2), p 212-218.
14. A.A. El-Rashidy, J.A. Roether, L. Harhaus, U. Kneser, and A.R. Boccaccini, Regenerating Bone with Bioactive Glass Scaffolds: A Review of in Vivo Studies in Bone Defect Models, *Acta Biomater.*, 2017, **62**, p 1-28. <https://doi.org/10.1016/j.actbio.2017.08.030>
15. M. Fabert, N. Ojha, E. Erasmus, M. Hannula, M. Hokka, J. Hyttinen, J. Rocherullé, I. Sigalas, and J. Massera, Crystallization and Sintering of Borosilicate Bioactive Glasses for Application in Tissue Engineering, *J. Mater. Chem. B*, 2017, **5**(23), p 4514-4525.
16. O.P. Filho, G.P. Latorre, and L.L. Hench, Effect of Crystallization on Apatite-Layer Formation of Bioactive Glass 45S5, *J. Biomed. Mater. Res.*, 1996, **30**(4), p 509-514.
17. V. Cannillo and A. Sola, Different Approaches to Produce Coatings with Bioactive Glasses: Enamelling vs Plasma Spraying, *J. Eur. Ceram. Soc. Elsevier*, 2010, **30**(10), p 2031-2039. <https://doi.org/10.1016/j.jeurceramsoc.2010.04.021>
18. J Chang and YL Zhou. (2018) Surface Modification of Bioactive Glasses, *Bioactive Glasses* Elsevier, 119-143, <https://doi.org/10.1016/B978-0-08-100936-9.00008-3>.
19. M.H. Fathi and A.D. Mohammadi, Preparation and characterization of sol-gel bioactive glass coating for improvement of biocompatibility of human body implant, *Mater. Sci. Eng. A*, 2008, **474**(1-2), p 128-133.
20. S.A. Omar, J. Ballarre, Y. Castro, E. Martinez Campos, W. Schreiner, A. Durán, and S.M. Cere, 58S and 68S Sol-Gel Glass-like Bioactive Coatings for Enhancing the Implant Performance of AZ91D Magnesium Alloy, *Surf. Coatings Technol.*, 2020, **400**, p 126224.
21. S. Heise, M. Höhlinger, Y.T. Hernández, J.J.P. Palacio, J.A. Rodríguez Ortiz, V. Wagener, S. Virtanen, and A.R. Boccaccini, Electrophoretic Deposition and Characterization of Chitosan/Bioactive Glass Composite Coatings on Mg Alloy Substrates, *Electrochim. Acta*, 2017, **232**, p 456-464.
22. K. Kawaguchi, M. Iijima, T. Murguruma, K. Endo, and I. Mizoguchi, Effects of Bioactive Glass Coating by Electrophoretic Deposition on Esthetical, Bending, and Frictional Performance of Orthodontic Stainless Steel Wire, *Dent. Mater. J.*, 2020, **39**(4), p 593-600. <https://doi.org/10.4012/dmj.2019-085>
23. M. Alaei, M. Atapour, and S. Labbaf, Electrophoretic Deposition of Chitosan-Bioactive Glass Nanocomposite Coatings on AZ91 Mg Alloy for Biomedical Applications, *Prog. Org. Coatings*, 2020, **147**, 105803. <https://doi.org/10.1016/j.porgcoat.2020.105803>
24. B. Garrido, I.G. Cano, and S. Dosta, Adhesion Improvement and in Vitro Characterisation of 45S5 Bioactive Glass Coatings Obtained by Atmospheric Plasma Spraying, *Surf. Coatings Technol.*, 2021, **405**, 126560.
25. E. Cañas, M.J. Orts, A.R. Boccaccini, and E. Sánchez, Solution Precursor Plasma Spraying (SPSS): A Novel and Simple Process to Obtain Bioactive Glass Coatings, *Mater. Lett.*, 2018, **223**, p 198-202.
26. A. Papyrin, V. Kosarev, S. Klinkov, A. Alkimov, and V. Fomin, (2007), Discovery of the Cold Spray Phenomenon and Its Basic Features, *Cold Spray Technol.*, 1-32. <https://doi.org/10.1016/B978-008045155-8/50001-6>
27. S.T. Oyinbo, and T.C. Jen, A Comparative Review on Cold Gas Dynamic Spraying Processes and Technologies, *Manuf. Rev.*, 2019, **6**, p 25. <https://doi.org/10.1051/mfreview/2019023>
28. P Vuoristo, (2014) Thermal Spray Coating Processes, *Comprehensive Materials Processing*, S. Hashmi, Ed., Elsevier, 229-276, <https://doi.org/10.1016/B978-0-08-096532-1.00407-6>.
29. R.N. Raolison, Y. Xie, T. Sapanathan, M.P. Planche, R. Kromer, S. Costil, and C. Langlade, Cold Gas Dynamic Spray Technology: A Comprehensive Review of Processing Conditions for Various Technological Developments till to Date, *Add. Manuf.*, 2018, **19**, p 134-159. <https://doi.org/10.1016/j.addma.2017.07.001>
30. V.K. Champagne, The Cold Spray Materials Deposition Process, The Cold Spray Materials Deposition Process: Fundamentals and Applications, *Woodhead Publishing Limited*, 2007 <https://doi.org/10.1533/9781845693787>
31. L.L. Hench, (2006) The Story of Bioglass®, *J. Mater. Sci.: Mater. Med.*
32. Y. Torres, C. Romero, Q. Chen, G. Pérez, J.A. Rodríguez-Ortiz, J.J. Pavón, L. Álvarez, C. Arévalo, and A.R. Boccaccini, “Electrophoretic Deposition of PEEK/45S5 Bioactive Glass Coating on Porous Titanium Substrate: Influence of Processing Conditions and Porosity Parameters,” *Key Engineering Materials*, T. Ebel and F. Pyczak, Eds., (Lüneburg, Germany), Trans Tech Publications, 2016, p 343-350.
33. S. Seuss, M. Heinloth, and A.R. Boccaccini, Development of Bioactive Composite Coatings Based on Combination of PEEK, Bioactive Glass and Ag Nanoparticles with Antibacterial Properties, *Surf. Coatings Technol.*, 2016, **301**, p 100-105.
34. B. Garrido, V. Albaladejo-Fuentes, I.G. Cano and, S. Dosta, Development of Bioglass/PEEK Composite Coating by Cold Gas Spray for Orthopedic Implants, *J. Therm. Spray Technol.*, 2022, **31**, p 186.
35. Y.C. Yang and E. Chang, Influence of Residual Stress on Bonding Strength and Fracture of Plasma-Sprayed Hydroxyapatite Coatings on Ti-6Al-4V Substrate, *Biomaterials*, 2001, **22**(13), p 1827-1836.
36. H.S. Hedia, Effect of Coating Thickness and Its Material on the Stress Distribution for Dental Implants, *J. Med. Eng. Technol.*, 2007, **31**(4), p 280-287.
37. A.M. Vilardell, N. Cinca, N. Garcia-Giralt, S. Dosta, I.G. Cano, X. Nogués, and J.M. Guilemany, In-Vitro Comparison of Hydroxyapatite Coatings Obtained by Cold Spray and Conventional Thermal Spray Technologies, *Mater. Sci. Eng. C*, 2020, **107**, 110306. <https://doi.org/10.1016/j.msec.2019.110306>
38. F.E. Ciraldo, E. Boccardi, V. Melli, F. Westhauser, and A.R. Boccaccini, Tackling Bioactive Glass Excessive in Vitro Bioreactivity: Preconditioning Approaches for Cell Culture Tests, *Acta Biomater.*, 2018, **75**, p 3-10.
39. Y. Xu and I.M. Hutchings, Cold Spray Deposition of Thermoplastic Powder, *Surf. Coatings Technol.*, 2006, **201**(6), p 3044-3050. <https://doi.org/10.1016/j.surfcoat.2006.06.016>
40. S.M. Kurtz and J.N. Devine, PEEK Biomaterials in Trauma, Orthopedic, and Spinal Implants, *Biomaterials*, 2007, **28**(32), p 4845-4869. <https://doi.org/10.1016/j.biomaterials.2007.07.013>
41. P. Patel, T.R. Hull, R.W. McCabe, D. Flath, J. Grasmeyer, and M. Percy, Mechanism of Thermal Decomposition of Poly(Ether Ether Ketone) (PEEK) from a Review of Decomposition Studies, *Polym. Degrad. Stab.*, 2010, **95**(5), p 709-718. <https://doi.org/10.1016/j.polymdegradstab.2010.01.024>

42. D. Bellucci, V. Cannillo, and A. Sola, An Overview of the Effects of Thermal Processing on Bioactive Glasses, *Sci. Sinter.*, 2010, **42**(3), p 307-320.
43. L. Lefebvre, J. Chevalier, L. Gremillard, R. Zenati, G. Thollet, D. Bernache-Assolant, and A. Govin, Structural Transformations of Bioactive Glass 45S5 with Thermal Treatments, *Acta Mater.*, 2007, **55**(10), p 3305-3313.
44. L.L. Hench, Chronology of Bioactive Glass Development and Clinical Applications, *New J. Glas. Ceram.*, 2013, **3**(02), p 67-73.
45. O. Peitl, E. Dutra Zanotto, and L.L. Hench, Highly Bioactive P2O5-Na2O-CaO-SiO2glass-Ceramics, *J. Non Cryst. Solids*, 2001, **292**(1–3), p 115-126.
46. M.A. Ur Rehman, F.E. Bastan, Q. Nawaz, W.H. Goldmann, M. Maqbool, S. Virtanen, and A.R. Boccaccini, Electrophoretic Deposition of Lawsonite Loaded Bioactive Glass (BG)/Chitosan Composite on Polyetheretherketone (PEEK)/BG Layers as Antibacterial and Bioactive Coating, *J. Biomed. Mater. Res. Part A*, 2018, **106**(12), p 3111-3122.
47. S. Yu, K.P. Hariram, R. Kumar, P. Cheang, and K.K. Aik, In Vitro Apatite Formation and Its Growth Kinetics on Hydroxyapatite/ Polyetheretherketone Biocomposites, *Biomaterials*, 2005, **26**(15), p 2343-2352.
48. D. Vukajlovic, K. Novakovic, and O. Bretcanu, Self-Crystallisation, an Unexpected Property of 45S5 Bioglass®, *Chem. Commun.*, 2021, **57**(99), p 13558-13561.
49. J.L. Ong and D.C.N. Chan, Hydroxyapatite and Their Use as Coatings in Dental Implants: A Review, *Crit. Rev. Biomed. Eng.*, 2000, **28**(5-6), p 667-707.
50. G. Bolelli, V. Cannillo, R. Gadow, A. Killinger, L. Lusvarghi, and J. Rauch, Microstructural and in Vitro Characterisation of High-Velocity Suspension Flame Sprayed (HVSFS) Bioactive Glass Coatings, *J. Eur. Ceram. Soc.*, 2009, **29**, p 2249-2257.
51. S. Bano, I. Ahmed, D.M. Grant, A. Nommeots-Nomm, and T. Hussain, Effect of Processing on Microstructure, Mechanical Properties and Dissolution Behaviour in SBF of Bioglass (45S5) Coatings Deposited by Suspension High Velocity Oxy Fuel (SHVOF) Thermal Spray, *Surf. Coatings Technol.*, 2019, **372**, p 229-238.
52. L.L. Hench and Ö. Andersson, Bioactive Glasses, *An Introduction to Bioceramics*, 1993 https://doi.org/10.1142/9789814317351_0003
53. J. Waser-Althaus, A. Salamon, M. Waser, C. Padeste, M. Kreutzer, U. Pieleles, B. Müller, and K. Peters, Differentiation of Human Mesenchymal Stem Cells on Plasma-Treated Polyetheretherketone, *J. Mater. Sci. Mater. Med.*, 2014, **25**(2), p 515-525.
54. X. Gu, X. Sun, Y. Sun, J. Wang, Y. Liu, K. Yu, and Y. Zhou, Bioinspired Modifications of PEEK Implants for Bone Tissue Engineering, *Front. Bioeng. Biotechnol.*, 2021, **8**, p 631616.
55. W. Hong, F. Guo, J. Chen, X. Wang, X. Zhao, and P. Xiao, Bioactive Glass–Chitosan Composite Coatings on PEEK: Effects of Surface Wettability and Roughness on the Interfacial Fracture Resistance and in Vitro Cell Response, *Appl. Surf. Sci.*, 2018, **440**, p 514-523.
56. M.B. da Cruz, J.F. Marques, G.M. Peñarrieta-Juanito, M. Costa, J.C.M. Souza, R.S. Magini, G. Miranda, F.S. Silva, J.M.M. Caramês, and A.D.S.P. da Mata, Bioactive-Enhanced Polyetheretherketone Dental Implant Materials: Mechanical Characterization and Cellular Responses, *J. Oral Implantol.*, 2021, **47**(1), p 9-17. <https://doi.org/10.1563/aaid-joi-D-19-00172>
57. Y. Deng, P. Zhou, X. Liu, L. Wang, X. Xiong, Z. Tang, J. Wei, and S. Wei, Preparation, Characterization, Cellular Response and in Vivo Osseointegration of Polyetheretherketone/Nano-Hydroxyapatite/Carbon Fiber Ternary Biocomposite, *Coll. Surf. B Biointerfaces*, 2015, **136**, p 64-73.

Publisher's Note Springer Nature remains neutral with regard to jurisdictional claims in published maps and institutional affiliations.